Physics Letters B 785 (2018) 626–630

Contents lists available at ScienceDirect

Physics Letters B

www.elsevier.com/locate/physletb

Proton-η' interactions at threshold

A.V. Anisovich [a,b], V. Burkert [c], M. Dugger [d], E. Klempt [a,c,*], V.A. Nikonov [a,b], B.G. Ritchie [d], A.V. Sarantsev [a,b], U. Thoma [a]

[a] Helmholtz-Institut für Strahlen- und Kernphysik, Universität Bonn, Germany
[b] NRC "Kurchatov Institute", PNPI, Gatchina 188300, Russia
[c] Thomas Jefferson National Accelerator Facility, Newport News, VA 23606, United States of America
[d] Arizona State University, Tempe, AZ 85287-1504, United States of America

ARTICLE INFO

Article history:
Received 19 March 2018
Received in revised form 14 June 2018
Accepted 14 June 2018
Available online 19 June 2018
Editor: D.F. Geesaman

Keywords:
Baryon spectroscopy
Meson photoproduction
Polarization observables

ABSTRACT

Recent data on photoproduction of η' mesons off protons have been included in the data base for the Bonn–Gatchina partial wave analysis. The real and imaginary parts of the S-wave $\eta' p \to \eta' p$ scattering amplitude in the threshold region were fit to yield the $\eta' p$ scattering length and the interaction range. This new analysis found $|a_{\eta' p}| = (0.403 \pm 0.015 \pm 0.060)$ fm and a phase $\phi = (87 \pm 2)^\circ$, while the range parameter is not well-constrained. The striking behavior of the GRAAL data on the beam asymmetry in the threshold region suggests that a narrow proton-η' resonance might exist. However, the scattering length was found to be relatively insensitive to the possible existence of this narrow resonance.

The interaction of the η' meson with the nucleon is a very active area of research at present, both in theoretical attempts to understand the interaction and in experiments aimed at providing polarization observables. The η'-meson is a member of the nonet of ground-state pseudoscalar mesons. Unlike other meson nonets, the η'-meson within the pseudoscalar nonet is nearly a pure SU(3) singlet state and may even contain contributions from a pseudoscalar glueball [1–6]. The octet of pseudoscalar mesons plays the role of Goldstone bosons; in the chiral limit of QCD when the quark masses go to zero, their masses vanish as well. The topological structure of the QCD vacuum breaks the so-called $U_A(1)$ symmetry [7], and the mass of the SU(3) singlet state, and hence the η' mass, does not vanish even for massless quarks.

Nevertheless, a sizable fraction of the η' mass is still due to chiral symmetry breaking. A key problem in non-perturbative QCD is whether the chiral symmetry can partially be restored in a strongly interacting environment [8–10]. If so, then the partial restoration of chiral symmetry should lead to a reduction of the η' mass, opening the possibility of the existence of $\eta' N$ bound states in nuclear matter. Even the existence of an η'-deuteron bound state in vacuum has been suggested [11]. A very recent determination of the η'-nucleus potential gave – with carbon [12] or niobium [13] as nuclei – a shallow potential of $-39 \pm 7_{\rm stat} \pm 15_{\rm syst}$ MeV [14] for η'-mesons with momentum of 1200–2900 MeV/c. A new determination of the η'-nucleus potential with a mean η' momentum of 600 MeV/c is in progress [15]. The scattering length $a_{p\eta'}$ and the range R of the η'-proton interaction also are directly related to the existence of any $\eta' N$ bound states, as well. In that regard, the η'–p scattering length has been determined by the COSY-11 Collaboration from the rise of the total cross section for the reaction $p + p \to p + p + \eta'$ [16].

In this letter we report a determination of the S-wave $\eta' p$ length from an analysis of data on the reaction

$$\gamma p \to \eta' p \tag{1}$$

This new analysis includes the recently-obtained data on the beam asymmetry Σ [17,18] for the η' photoproduction process, as well as the recent high-precision data on the differential cross for this reaction [19]. The data from GRAAL show a beam asymmetry that is larger near threshold ($W = 1896$–1910) than the value for that observable in the very next measured energy bin ($W = 1910$–1917). The difference in the measured asymmetries is especially striking when one considers that the difference between the centers of those two energy bins is a mere 10 MeV. In a partial-wave analysis, this remarkable behavior suggests the existence of a narrow resonance at the $\eta' p$ threshold.

Data on the $\gamma p \to \eta' p$ reaction were analyzed recently with the aim of identifying the contributions to this reaction from different N^* resonances, and to determine the $N^* \to N\eta'$ branching ratios [20]. Four resonances, $N(1895)1/2^-$, $N(1900)3/2^+$,

* Corresponding author.
E-mail address: klempt@hiskp.uni-bonn.de (E. Klempt).

https://doi.org/10.1016/j.physletb.2018.06.034

$N(2100)1/2^+$, and $N(2120)3/2^-$, were found to provide the most significant contributions. The fit used the differential cross sections $d\sigma/d\Omega$ from the Crystal Barrel [21] and CLAS [22] experiments, along with recent beam asymmetry data from GRAAL Σ [17] and CLAS Σ [18] mentioned above. In the analysis presented here, we also used the new precise MAMI-A2 data on the $\gamma p \to \eta' p$ differential cross section [19]. In addition to the data on η' photoproduction, a large body of pion and photo-induced reactions is fit in a coupled channel analysis. The data base includes the real and imaginary part of the πN scattering amplitude for the partial waves up to $J = 9/2^{\pm}$ from Ref. [23] and data on pion and photoproduction with πN, ηN, $K\Lambda$, $K\Sigma$, $N\pi^0\pi^0$, and $N\pi^0\eta$ in the final state. A list of the data with references can be found on our web page (pwa.hiskp.uni-bonn.de/).

Similar fits – even though mostly restricted to the $\gamma N \to \eta' N$ reaction – have recently been presented in Refs. [24–27]. In Ref. [24], a quark model is used to fit differential cross sections for η' photoproduction off protons [21,22] and neutrons [28]; Ref. [25] includes data on cross sections for $\pi^- p \to \eta' n$ and on $NN \to NN\eta'$ [29] (references to $\pi^- p$ and earlier NN data can be found in Ref. [25]). The authors of Ref. [27] fit CLAS 2009 differential cross sections [22] and the total cross section from MAMI-A2 collaboration [19] within an isobar model. The analyses [20,24,25,27] agree that nucleon resonances should be included even though there is no consensus concerning the spin-parities of the preferred resonances. No explicit resonances were included in the analysis presented in Ref. [26], but instead final-state interactions between η' mesons and nucleons were studied within a three-flavor linear σ model. The need of final-state interactions is demonstrated even though the quality of the fit is moderate. The recent CLAS data on the $\gamma p \to \eta' p$ beam asymmetry, which include a much wider energy range than that provided by GRAAL, [18] have to date only been included in Ref. [20].

The formalism used here to fit the data is described in Ref. [20]. We recall here that for the reaction $\gamma p \to \eta' p$, the coupling constants in the initial and the final state are weak and in most cases one can neglect contributions of these channels to the rescattering sequence taking them into account only once. Then the amplitude

$$A^h_f = \hat{G}_f + \hat{P}_a[(\hat{I} - \hat{B}\hat{K})^{-1}\hat{B}]_{ab}\hat{D}_{bf} \tag{2}$$

can be used. The K-matrix elements describe the transition between K-matrix channels a and b:

$$\hat{K}_{ab} = \sum_\alpha \frac{g^{(\alpha)}_a g^{(\alpha)}_b}{M^2_\alpha - s} + f_{ab} \tag{3}$$

where M_α are masses of the K-matrix poles, $g^{(\alpha)}_a$ is the couplings of the pole α to the channel a and the terms f_{ab} describe the nonresonant transition between the channels a and b.

The transition from the initial γN state to the K-matrix channel a is represented by the P-vector:

$$\hat{P}_a = \sum_\alpha \frac{g^{(\alpha)}_{\gamma N} g^{(\alpha)}_a}{M^2_\alpha - s} + F_a \tag{4}$$

where $g^{(\alpha)}_{\gamma N}$ are resonance couplings to the γN channel and the F_a describe non-resonant transitions. The matrix D

$$\hat{D}_{bf} = \sum_\alpha \frac{g^{(\alpha)}_b g^{(\alpha)}_f}{M^2_\alpha - s} \tag{5}$$

represents the transition from the channel b to the final state 'f'. $\hat{G}_f$ stands for the transition from γN to $\eta' p$ in the final state:

$$\hat{G}_f = \sum_\alpha \frac{g^{(\alpha)}_{\gamma N} g^{(\alpha)}_f}{M^2_\alpha - s} \tag{6}$$

$\hat{\mathbf{B}}$ is a diagonal matrix with an imaginary part given by the corresponding phase space volume

$$\hat{B}_i = \Re e B_i + i\rho_i\,, \tag{7}$$

where $\Re e B_i$ is calculated from the dispersion integral with one subtraction regularization. The decay couplings $g^{(\alpha)}_f$ were fitted as free parameters. If the final channel is treated as the K-matrix channel the eq. (2) reduced to the standard P-vector amplitude:

$$A^h_f = \hat{P}_a(\hat{I} - \hat{B}\hat{K})^{-1}_{af} \tag{8}$$

The parametrization (8) was used for the description of the S_{11} partial wave where the opening of the $\eta' p$ channel is responsible for the cusp effect in the $\gamma p \to \eta p$ total cross section and should be taken explicitly into account. The forward peak in the differential cross section at high energies is described by a Reggeized $\rho(\omega)$-meson exchange amplitude [31,32].

The fit solution presented in Ref. [20] predicted reasonably well the new MAMI-A2 data [19] on the differential cross section for $\gamma p \to \eta' p$. Indeed, inclusion of that new MAMI-A2 data in a new fit did not change the resonance content contributing to η' photoproduction, and the changes in the $N\eta'$ decay branching ratios found in a fit including the new MAMI-A2 data were found to be small. The uncertainties for model parameters found in Ref. [20] were dominated by those uncertainties arising due to variations of the model assumptions. On the whole, inclusion of the new MAMI-A2 data does stabilize the amplitudes near the η' photoproduction threshold. In the present paper, the fit of Ref. [20] including the new MAMI-A2 data will be the baseline from which we explore the inclusion of the beam asymmetry data from GRAAL [17] and CLAS [18]. In what follows, we will refer to this baseline fit as our "standard fit".

Fig. 1 shows the GRAAL [17] and CLAS [18] data on the beam asymmetry Σ, while Fig. 2 gives differential cross section measured at MAMI-A2 [19]. The uncertainties represent the statistical errors; the systematic errors are supposed to change the absolute values only, independent of the invariant mass. A global normalization factor is admitted but restricted by the systematic uncertainty.

The data are compared to two fits:

1. Our *standard fit* is represented by the solid curves. This standard fit gives a reasonable description of the data except for the region just above the threshold. This fit predicts a vanishing beam asymmetry for the mass range where the GRAAL data exist, and a relatively flat angular distribution for the differential cross section. However, in contrast to the predictions of this standard fit, the GRAAL data show an appreciably beam asymmetry at threshold, and the new MAMI-A2 data indicate a significant forward rise of the differential cross section in the 1899.5 to 1902.7 MeV mass range. The fit probability for the low-energy region is small: it is for the first three bins in the beam asymmetry Σ was 5% and less than 1% for the first six bins in the cross sections $d\sigma/d\Omega$.

2. We tried to improve the *standard fit* by including a narrow resonance with $N\eta'$ as only decay mode. When decays of the narrow resonance to $N\pi$ or to $p\eta$ were admitted, the coupling constants were fitted to zero. The narrow resonance was represented by a convolution of a squared Breit–Wigner amplitude and a Gaussian function representing the resolution. The GRAAL resolution was fixed to 16 MeV (FWHM), for the MAMI-A2 data the resolution is expected to be given by the bin width (which corresponds to $\sigma \approx 3.2/\sqrt{12} \approx 1$ MeV), and is neglected. The narrow

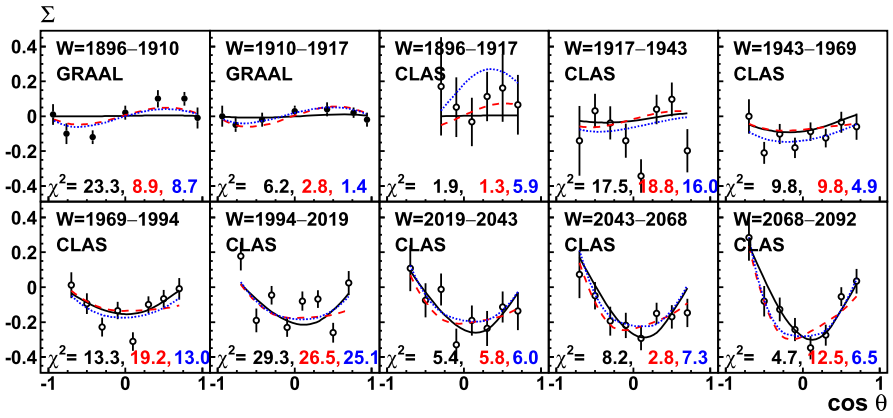

Fig. 1. (Color online.) The beam asymmetry Σ for the reaction $\gamma p \to \eta' p$. Shown are data from GRAAL [17] and recent data from CLAS [18]. The curves represent three fits: the solid (black) curve represents the main fit without a new narrow resonance. The fit that includes a narrow $\eta' p$ threshold resonance with spin-parity $J^P = 3/2^-$ ($J^P = 5/2^-$) is shown by dashed (red) curves, for $J^P = 5/2^-$ by dotted (blue) curves. The curves for the CLAS beam asymmetries are scaled by a factor 0.94 (see Ref. [20]). The numbers shown as inserts in the subfigures give the χ^2 contribution of the data for the fit without a narrow $\eta' p$ resonance and for the fits which includes a narrow resonance with $J^P = 3/2^-/J^P = 5/2^-$ (red/blue).

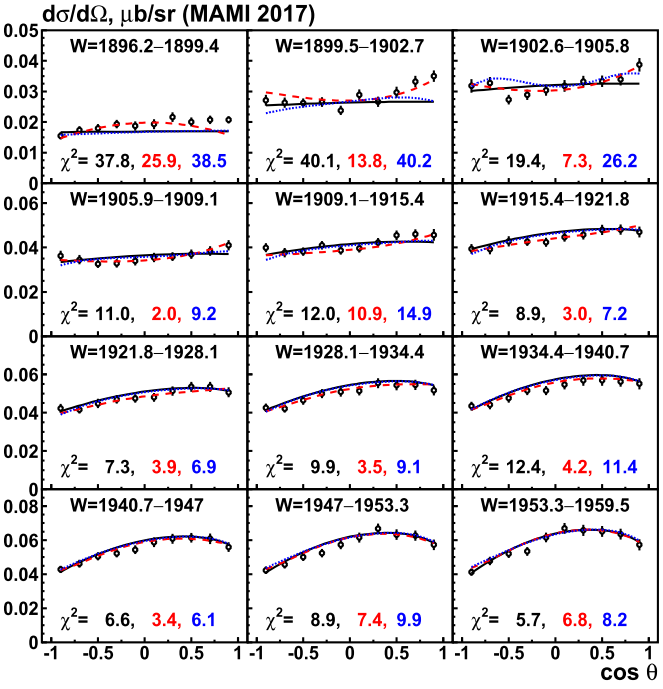

Fig. 2. (Color online.) The MAMI-A2 differential cross section for $\gamma p \to \eta' p$ [19] and three BnGa fits. The dashed (red) – or dotted (blue) – curves represent fits which include a narrow $\eta' p$ threshold resonance with spin-parity $J^P = 3/2^-$ or $5/2^-$, the solid curve the main fit without a narrow resonance. The numbers shown as inserts in the subfigures give the χ^2 contribution of the data for the fit without a narrow $\eta' p$ resonance (black) and for the fits which include a narrow resonance with $J^P = 3/2^-$ (red) $J^P = 5/2^-$ (blue).

resonance requires four additional parameters: M, Γ, and the product of helicities $A_{1/2}, A_{3/2}$ and the square root of the $N\eta'$ decay branching fraction.

For the first two bins in Fig. 1, the beam asymmetry was calculated for 1 MeV wide bins and then averaged. For the other bins, the beam asymmetries were calculated for the central masses. Different spin-parity combinations were tested: $J^P = 1/2^\pm, 3/2^\pm, 5/2^\pm, 7/2^\pm$. Fits with $J^P = 1/2^\pm$ and $J^P = 7/2^\pm$ gave no improvement; the best fit was achieved with quantum numbers $J^P = 3/2^-$. The fit probability increased to 75% (15%) for Σ ($d\sigma/d\Omega$) in the low-energy region. Spin-parity $5/2^-$ could also be possible, the fit probability was 50% ($\leq$1%). The dashed curves in Figs. 1 show this fit. Assuming $J^P = 3/2^-$, the fit returns

$$M_{\eta' p} = 1900 \pm 1\,\text{MeV};\ \ \Gamma_{\eta' p} < 3\,\text{MeV}. \tag{9}$$

When the narrow resonance is included, the χ^2 of the fit improves from 120.3 to 59.9 for the 70 data points in the first five Mainz mass bins, or from 29.5 to 11.7 for the 14 GRAAL data points. Due to the strongly rising phase space, the narrow resonance entails a small $J^P = 3/2^-$ amplitude extending over more than 10 MeV. Note that the mass resolution is given by the photon beam energy and not by the reconstruction of the final state.

The existence of such a narrow resonance in the D-wave is unexpected. (In the S-wave, a $N\eta'$ bound state just below the threshold is predicted in the linear sigma model [30].) To trace the origin of the narrow structure, we have excluded the MAMI-A2 data from the fit. If we impose the GRAAL resolution of 16 MeV (FWHM), the narrow width is confirmed. Decreasing the resolution leads to a larger natural width of the narrow resonance. Thus, the evidence for the narrow width of the resonance rests mostly on the MAINZ $\gamma p \to \eta' p$ differential cross section [19].

The GRAAL data suggest the possible existence of a $p\eta'$ threshold resonance; the MAMI-A2 differential cross sections support this conjecture. Hence we think that the search for a narrow $N\eta'$ resonance should be continued with new data with high statistics and precision. A measurement of further polarization observables might help to find an unambiguous answer. The observables for which predictions are made include those for several polarized-photon-beam/polarized-proton-target combinations.

Fig. 3 shows the predictions for the polarization observables E, H, P and T for a 2 MeV mass region at the nominal mass of the possible $\eta' p$ resonance. The observable E is the (normalized) difference between the meson photoproduction cross sections for helicity 1/2 and helicity 3/2. The observable H is the correlation between linearly-polarized photons and transversely-polarized protons. The observable P is the polarization of the outgoing proton with respect to the scattering plane. The observable T is the asymmetry in the production cross section when the target proton polarization transverse to the incident photon beam is flipped.

When a resonance is added to the fit, significant differences in one or more of these observables should arise. In particular, data for P and H should indicate the presence of a resonance (even if the resonance is narrow) if such a structure exists, and predictions for those observables are relatively sensitive to the presence of that state. However, we also recognize that experiments so near

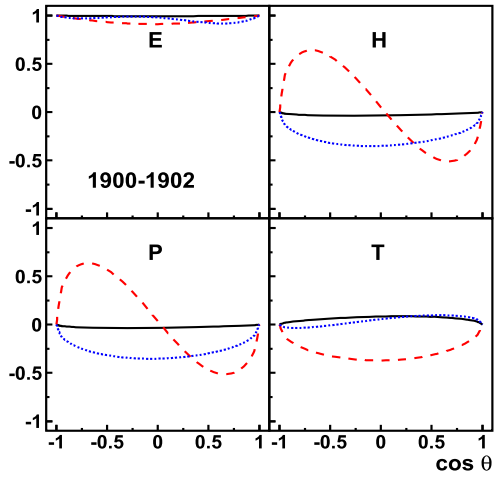

Fig. 3. (Color online.) Prediction for the double-polarization observables E, G, P and T for the 1901–1902 MeV mass window. The solid (black) curve represents the main fit without a new narrow resonance, the dashed (red) and dotted (blue) curves represent the predictions for the case when a narrow $\eta' p$ threshold resonance with spin-parity $J^P = 3/2^-$ or $5/2^-$ exists.

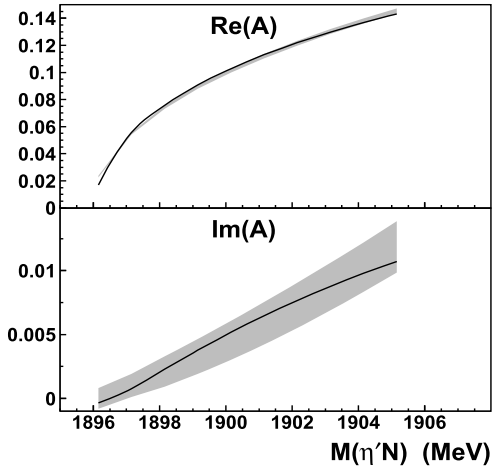

Fig. 4. Real part (upper panel) and imaginary part (lower panel) of the $\eta' N \to \eta' N$ S-wave scattering amplitude A (solid curve) using Eqn. (10). The phase is rotated to have a vanishing imaginary part at the $\eta' p$ threshold. The error band is calculated from the variance of the partial-wave analysis coefficients.

to threshold are very demanding, especially if a putative resonance is so narrow that the polarization observables can only show evidence for that resonance in a small mass window.

We now turn to the main objective of this paper: the determination of the $\eta' p$ scattering length. The scattering length is given by the $J^P = 1/2^-$-(S_{11})-wave amplitude for $\eta' p$ production at the η' threshold (corresponding to the wave in which the $\eta' p$ orbital angular momentum vanishes). As the primary solution, we use the *standard fit* without additional narrow resonance. The upper and lower panels of Fig. 4 show the real and imaginary parts, respectively, of the S_{11} partial wave in the low-energy region, from the threshold to 10 MeV above. The fit solution provides the real and imaginary part of the S_{11} amplitude as a function of $M_{\gamma p}$. The statistical uncertainties are unrealistically small; therefore we determine the uncertainties from a series of fits where a high-mass resonance with a mass in the 2.2 to 2.5 GeV mass range and with spin-parity $J^P = 1/2^{\pm}, 3/2^{\pm}, 5/2^{\pm}$ or $7/2^{\pm}$ is added to the set of resonances used in the *standard fit*. From the spread of the results we calculate error bands for the real and imaginary part of the S_{11} amplitude that are shown in Figs. 4a and b.

A first fit (not shown) to the squared amplitude with $\beta \cdot \sqrt{s - s_0}$ and β and s_0 as free parameters yields an offset of 1896.0 ± 1.0 MeV, fully consistent with the sum of proton and η' mass: 1896.05 ± 0.06 MeV.

The results on the real and imaginary part of the S_{11} amplitude (Figs. 4a and b) were fit with a function [33]

$$A = \frac{a\,k}{1 - i\,k\,a + R\,k^2\,a/2 + d\,k^4\,a} \tag{10}$$

$$k = \frac{\sqrt{(s - (M_p + M\eta')^2)(s - (M_p - M_{\eta'})^2)}}{2\sqrt{s}}$$

where $a = a_{p\eta'}$ is the $\eta' p$ scattering length, R the range of the $\eta' p$ interaction, d a parameter representing higher-order terms, $\sqrt{s} = M_{\eta' p}$ the invariant mass, and k the η' momentum in the $\eta' p$ rest frame. The fit to Figs. 4a and b give consistent results for the modulus of the $\eta' p$ scattering length.

The S_{11} amplitude has one arbitrary phase which cannot be defined from experiment. The phase could be defined as zero at the pion-production threshold or, alternatively, at the η' production threshold. In the fits, the phase is defined relative to η' production threshold.

We fit the amplitude in the range from threshold to 10 MeV above the threshold, the parameter d was fixed to zero or was used as a free fit parameter. From these fits, we obtained a modulus of the scattering length in the range $0.367 > |a_{p\eta'}| > 0.344$ fm with a statistical uncertainty (σ) of less than ± 0.013 fm. Then we performed fits with an additional narrow resonance, again with $d = 0$ and with d as free fit parameter. In this case the fit returned values between $0.462 > |a_{p\eta'}| > 0.394$ fm and a statistical uncertainty of ± 0.020 fm. The modulus of the $\eta' p$ scattering length depends only weakly on the existence of a narrow D-wave resonance at the $\eta' p$ threshold. Since we do not know if a narrow resonance exists or not, we quote

$$|a_{p\eta'}| = (0.403 \pm 0.020 \pm 0.060)\ \text{fm} \tag{11}$$

as our final result, where the first uncertainty is statistical, the second one is nature. $\delta_{p\eta'} = (1.5 \pm 0.5)^\circ$. The phase shift between the πN and the $\eta' p$ threshold is rather stable. Relative to the pion-production threshold, we find a phase of

$$\delta_{N\pi} = (87 \pm 2)^\circ \tag{12}$$

at the $p\eta'$ threshold. These values are consistent with the numbers obtained at COSY [16]: $\text{Re}(a_{p\eta'}) = 0 \pm 0.43$ fm and $\text{Im}(a_{p\eta'}) = 0.37\ ^{+0.40}_{-0.16}$ fm.

The phase of about 90° implies that the real part of the scattering length is small compared to imaginary part. The existence of a $\eta' p$ (S-wave) bound state would require the real part to be larger than the imaginary part [34]. This value for the scattering length does not, however, exclude the existence of a $\eta' N$ bound state in a nuclear environment or the existence of a D-wave $\eta' N$ resonance.

The range parameter is a complex number which remained essentially undetermined. We find $R = (3.2 \pm 2.1) + i(1.6 \pm 1.2)$ fm for fits with $d = 0$ and $R = (10 \pm 5) + i(5 \pm 5)$ fm when d is varied freely. We might expect the range to be given by $f_0(500)$ exchange, i.e. $R \sim 0.4$ fm. The fit deteriorates only slightly when this value is imposed. There was wide variation of the estimates for the value of (and uncertainty for) d, so no specific value for that quantity is quoted here.

In all fits, $N\eta$ decay modes of most resonances are admitted. The opening of the $\eta' p$ threshold can be seen in the data as pointed out in Ref. [19]. The data are shown in Fig. 5 and compared

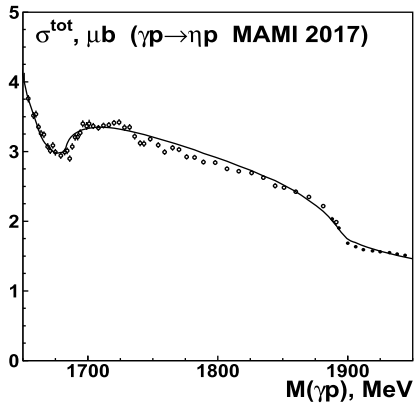

Fig. 5. Total cross section for $\gamma p \to \eta p$ Ref. [19]. The significant drop at the $\eta' p$ threshold near 1890 MeV indicates the presence of strong contributions from the $N(1895)1/2^-$ resonance. The data shown come from two running periods. The cross sections for the high-mass data above 1880 MeV have been scaled with a factor 1.06.

to the BnGa fit. The drop of the cross section at about 1890 MeV is due to the opening of the η' threshold and indicates the presence of a resonance at about this mass with quantum number $J^P = 1/2^-$.

Summarizing, we have studied the photoproduction reaction $\gamma p \to \eta' p$. The GRAAL data on the beam asymmetry for this reaction suggest the possible existence of a narrow $\eta' p$ resonance at 1900 ± 1 MeV and a width of less than 3 MeV. The $\eta' p$ scattering length has been determined. Its magnitude is found to be $|a_{p\eta'}| = (0.403 \pm 0.020 \pm 0.0600)$ fm, its phase relative to the πN threshold is $\delta = (87 \pm 2)^\circ$. This value does not depend on the existence or not of the narrow $\eta' p$ resonance. The range of the interaction could not be determined with a reasonable accuracy.

We would like to thank V. Metag for illuminating discussions on η' interactions in nuclei. This work was supported by the Deutsche Forschungsgemeinschaft (SFB/TR110). The work of AVA, AVS and VAN is supported by the RSF grant 16-12-10267. Work at Arizona State University was supported by the U. S. National Science Foundation under award PHY-1306737. This material is in part based upon work supported by the U.S. Department of Energy, Office of Science, Office of Nuclear Physics under contract DE-AC05-06OR23177.

References

[1] D. Coffman, et al., MARK-III Collaboration, Phys. Rev. D 38 (1988) 2695.
[2] T. Feldmann, P. Kroll, B. Stech, Phys. Rev. D 58 (1998) 114006.
[3] R. Escribano, Eur. Phys. J. C 65 (2010) 467.
[4] F.G. Cao, Phys. Rev. D 85 (2012) 057501.
[5] R. Aaij, et al., LHCb Collaboration, J. High Energy Phys. 1501 (2015) 024.
[6] L.A. Harland-Lang, V.A. Khoze, M.G. Ryskin, A.G. Shuvaev, Phys. Lett. B 770 (2017) 88.
[7] G. 't Hooft, Phys. Rev. D 14 (1976) 3432, Erratum: Phys. Rev. D 18 (1978) 2199.
[8] V. Bernard, U.G. Meissner, Nucl. Phys. A 489 (1988) 647.
[9] G.E. Brown, M. Rho, Phys. Rev. Lett. 66 (1991) 2720.
[10] T. Hatsuda, S.H. Lee, Phys. Rev. C 46 (1) (1992) R34.
[11] T. Sekihara, H. Fujioka, T. Ishikawa, Phys. Rev. C 97 (4) (2018) 045202.
[12] M. Nanova, et al., CBELSA/TAPS Collaboration, Phys. Lett. B 727 (2013) 417.
[13] M. Nanova, et al., CBELSA/TAPS Collaboration, Phys. Rev. C 94 (2) (2016) 025205.
[14] V. Metag, M. Nanova, E.Y. Paryev, Prog. Part. Nucl. Phys. 97 (2017) 199.
[15] M. Nanova, et al., CBELSA/TAPS Collaboration, The η'-carbon potential at low meson momenta, in preparation.
[16] E. Czerwinski, et al., Phys. Rev. Lett. 113 (2014) 062004.
[17] P. Levi Sandri, et al., Eur. Phys. J. A 51 (7) (2015) 77.
[18] P. Collins, et al., CLAS Collaboration, Phys. Lett. B 771 (2017) 213.
[19] V.L. Kashevarov, et al., Phys. Rev. Lett. 118 (21) (2017) 212001.
[20] A.V. Anisovich, et al., Phys. Lett. B 772 (2017) 247.
[21] V. Crede, et al., CBELSA/TAPS Collaboration, Phys. Rev. C 80 (2009) 055202.
[22] M. Williams, et al., CLAS Collaboration, Phys. Rev. C 80 (2009) 045213.
[23] R.A. Arndt, W.J. Briscoe, I.I. Strakovsky, R.L. Workman, Phys. Rev. C 74 (2006) 045205.
[24] X.H. Zhong, Q. Zhao, Phys. Rev. C 84 (2011) 065204.
[25] F. Huang, H. Haberzettl, K. Nakayama, Phys. Rev. C 87 (2013) 054004.
[26] S. Sakai, A. Hosaka, H. Nagahiro, Phys. Rev. C 95 (4) (2017) 045206.
[27] V.A. Tryasuchev, A.G. Kondratyeva, A.A. Kiziridi, Russ. Phys. J. 60 (5) (2017) 782.
[28] I. Jaegle, et al., CBELSA/TAPS Collaboration, Eur. Phys. J. A 47 (2011) 11.
[29] P. Klaja, et al., Phys. Lett. B 684 (2010) 11.
[30] S. Sakai, D. Jido, Hyperfine Interact. 234 (1–3) (2015) 71.
[31] A. Anisovich, E. Klempt, A. Sarantsev, U. Thoma, Eur. Phys. J. A 24 (2005) 111.
[32] A.V. Sarantsev, A.V. Anisovich, V.A. Nikonov, H. Schmieden, Eur. Phys. J. A 39 (2009) 61.
[33] A.M. Green, S. Wycech, Phys. Rev. C 71 (2005) 014001, Erratum: Phys. Rev. C 72 (2005) 029902.
[34] Q. Haider, L.C. Liu, Int. J. Mod. Phys. E 24 (10) (2015) 1530009.